Zhou *et al. Journal of Wood Science* (2022) 68:36
https://doi.org/10.1186/s10086-022-02045-2

Journal of Wood Science

ORIGINAL ARTICLE Open Access

# Study on in-plane shear failure mode of cross-laminated timber panel

Yuhao Zhou[1], Zhaoyu Shen[1], Haitao Li[2], Yao Lu[1] and Zheng Wang[1*]

**Abstract**

To explore in-plane shear failure mode of cross-laminated timber (CLT) panel, this paper carried out relevant research work from the perspective of stress analysis and combined with the crack morphology of the specimen after planar shear. In this study, the load–displacement curve of the hemlock [*Tsuga canadensis* (L.) Carrière] CLT specimen was obtained by a three-point bending test or an improved planar shear test, the crack morphology of the CLT vertical layer and the azimuth angle of the crack surface were observed and recorded synchronously. The shear strength values of CLT specimens under the two tests were obtained by corresponding calculation. Then the stress analysis of the CLT vertical layer was combined with the azimuth angle of the crack surface to discuss the failure mode of the CLT vertical layer in planar shear. The results showed that the planar shear strength measured by the three-point bending test and the improved planar shear test was in good agreement, and the results measured by the improved planar shear test were more dispersed than those measured by the three-point bending test; Considering the approximation that the in-plane shear of the CLT vertical layer could be treated as pure shear, the three-point bending test was better than the improved planar shear test; For the vertical layer of 63.3% CLT specimens, the azimuth of the crack surface was near the azimuth of the first principal plane obtained by stress analysis; There were two failure modes in the CLT vertical layer in-plane shear: tension failure and shear failure.

**Keywords:** Cross-laminated timber (CLT), In-plane shear, Three-point bending test, Improved planar shear test, Crack morphology, Stress circle, Failure mode

## Introduction

In recent years, in developed countries in Europe and the United States, sustainable bamboo-based materials [1, 2], passively controlled structural systems [3], as well as cross-laminated timber (CLT), a new type of building material made from sawn timber as the basic unit, have been widely used in the construction of mid-rise and high-rise residential and public buildings. CLT solves the height limitation of traditional wood structure buildings. It is not only easy to implement factory prefabrication and on-site assembly, but also has the advantages of good dimensional stability, sound insulation, good heat preservation performance, good mechanical properties, convenient construction, low carbon, carbon fixation, and environmental protection [4–6]. Although traditional CLT structures suffer high seismic damage in timber components (i.e., CLT walls) subjected to seismic actions, CLT structures are easy to repair after the earthquake [7, 8]. And new seismic devices devoted to avoiding high damage are being studied [9]. However, wood has orthotropic anisotropy material behavior, so the mechanical properties of materials composing the wood are undoubtedly complicated [10–13]. When CLT is used as a floor slab, beam, or other components that are subjected to out-of-plane lateral loads, the planar shear strength becomes one of the key factors to control the mechanical performance of CLT [14]. Therefore, it is particularly important to study the failure mode of CLT in-plane shear.

*Correspondence: wangzheng63258@163.com

[1] College of Materials Science and Engineering, Nanjing Forestry University, Nanjing 210037, China
Full list of author information is available at the end of the article

Since 2016, the main research topics on CLT have included the following areas: material structure, test methods, loading methods, and failure mechanisms of the CLT vertical layer. First, the research on the material structure applies the following tests: CLT three-point bending test, improved planar shear test, and four-point bending test. The test content is aimed at studying the influence of the number of CLT layers, the thickness of each layer, materials, and processing methods of the vertical and parallel layers on the rolling shear strength, shear modulus, and stiffness of CLT [15–18]. It should be noted that rolling shear refers to the shear strain behavior of timber in its cross-section. Under the action of shear force, cracks are easy to occur in the transition area of early and late wood, wood ray and pith. This failure is called rolling shear failure [19]. Second, the research on the test methods for testing CLT shear properties (rolling shear strength and shear modulus) includes the similarity of the three-point bending test and improved planar shear test, and the span-to-height ratio of the test piece [20, 21]. Third, the research on the loading methods includes the specimen damage under fatigue loading and the impact of damage accumulation on CLT rolling shear strength [22]. Fourth, the research on the failure mechanism of the CLT vertical layer includes the torque load test, Monte Carlo simulation, and simulation on the shear block specimen, which showed that the CLT rolling shear failure is brittle [23, 24].

In the previous research [25], the three-point bending test or the improved planar shear test was carried out on CLT specimen. The load–displacement curve of the specimen and the peak load value of the curve were obtained. When the test was over, the crack morphology of the damaged CLT vertical layer was recorded, and the azimuth angle of the crack surface was measured. These were used to reveal the appearance characteristics of the CLT vertical layer crack initiation and propagation on the load–displacement curve.

Based on the above research, the stress, strain, principal stress, maximum and minimum shear stress of the vertical layer of CLT specimens in CLT three-point bending test and improved planar shear test were analyzed in this study. It clarified that the vertical layer of the three-point bending specimen and the planar shear specimen could achieve in-plane shear, and could be approximately treated as pure shear. When considering the in-plane shear of the CLT vertical layer as pure shear, the three-point bending test was better than the improved planar shear test. Since the CLT vertical layer had undergone shear deformation in the cross-section of the vertical layer, the CLT vertical layer deformation was referred to as in-plane shear in this article, and the rolling shear term was not adopted. The corresponding strength value was called the CLT planar shear strength.

In brief, this study revealed the failure mechanism of CLT in-plane shear by combining the principal stress, maximum and minimum shear stress (including value and direction) of CLT vertical layer with the azimuth of crack surface, and put forward two failure modes of CLT in-plane shear: shear failure and tensile failure.

## Materials and methods

### Materials

CLT three-point bending and improved planar shear specimens were sawed from a 3-layered $500 \times 1200 \times 105$ mm hemlock [*Tsuga canadensis* (L.) Carrière] CLT panel. The component unit of the panel (hemlock timber) was rip-cut. The one-component polyurethane (PUR) was used as the adhesive, with the sizing amount of 180 g/m$^2$. The elasticity modulus of CLT major strength direction was $1.07 \times 10^4$ MPa, and the bending strength was 35 MPa. The above materials and relevant data were provided by Ningbo Sino-Canada Low-Carbon Technology Research Institute Co., Ltd., China.

#### *Specimen for the CLT three-point bending test*

The specimens of A-series were as follows: $735 \times 305 \times 105$ mm, 15 pieces, to achieve a three-point bending load with a span-to-height ratio of 6 (Fig. 1). The specimens of B-series were as follows: $735 \times 210 \times 105$ mm, 6 pieces, to achieve a three-point bending load with a span-to-height ratio of 6. The laminar width of the vertical layer of A, B-series was 140 mm. The average moisture content (MC) of A and B-series specimens was 12%, and the average density $\rho$ was 475 kg/m$^3$. The widths of A-series and B-series were 305 mm and 210 mm, respectively, to explore the influence of the width of the three-point bending specimens on the CLT planar shear (rolling shear) strength test value. It should be noted that the fiber orientation of the parallel layer is parallel to the length of the specimen, and the fiber orientation of the vertical layer is parallel to the width of the specimen.

#### *Specimen for the CLT-improved planar shear test*

The specimens of C-series were as follows: $270 \times 135 \times 105$ mm (the length of the specimen refers to the length of the interface between the vertical layer and the parallel layer), 9 pieces. The laminar width of the vertical layer of C-series was 140 mm. The average MC was 14%, and the average density $\rho$ was 431 kg/m$^3$. The design of the CLT-improved planar shear test is shown in Fig. 2. Compared with the planar shear test specified in EN408 [26] and ASTM D2718 [27], the advantage of the

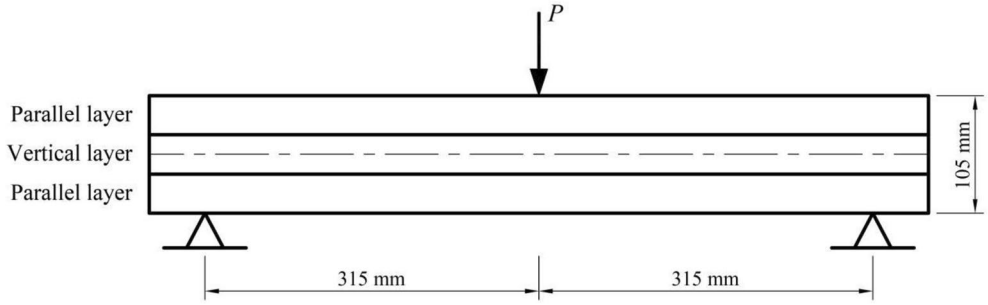


**Fig. 1** Schematic diagram of the CLT three-point bending test loading

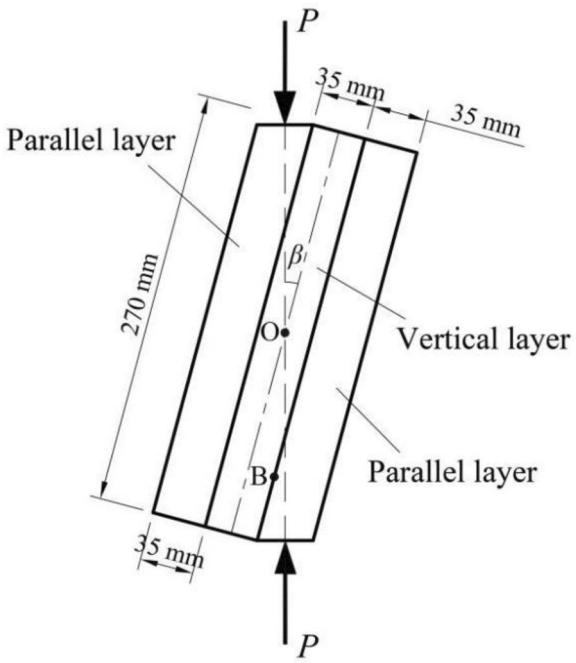


**Fig. 2** Schematic diagram of the CLT-improved planar shear test loading

improved planar shear test is that there's no need to paste steel plates on the surface of two parallel layers [28].

### Test method

JAW-2000 multi-channel structure test loading system (maximum test force of 300 kN) and AG-IC electronic universal mechanical testing machine (maximum test force of 100 kN) were used to carry out the three-point bending test and the improved planar shear test (Fig. 3). And the load–displacement curve of the specimen was obtained. The tests were carried out in displacement control by using supporting software, with a loading speed of 0.5 mm/min.

The process of the crack initiation and propagation on the test specimen was observed through video recording synchronized with the load–displacement curve. It was applied to explore the relationship between the initiation and propagation of crack and the characteristics of the load–displacement curve.

The maximum load value from the load–displacement curve was obtained to calculate the CLT planar shear strength $\tau$.

According to ASTM D198 [29], the formula used in the CLT three-point bending test is as follows:

$$\tau = 0.92\frac{3P_{\max}}{4bh}. \quad (1)$$

In Eq. 1: $\tau$ is the CLT planar shear strength, MPa; $P_{\max}$ is the maximum peak load, N; $b$ is the width of the specimen, mm; $h$ is the thickness of the specimen, mm.

It should be noted that 0.92 in Eq. 1 is the correction factor, which is determined by the location of the maximum interlayer shear stress of CLT panel. It is related to the number of layers of the panel [30].

According to EN 408 and reference [28], the formula used in the CLT-improved planar shear test is as follows:

$$\tau = \frac{P_{max}\cos\beta}{lb}. \quad (2)$$

In Eq. 2: $\tau$ is the CLT planar shear strength, MPa; $P_{\max}$ is the maximum peak load, N; $l$ is the length of the specimen, mm; $\beta$ is the inclination angle of the specimen, °.

The final crack morphology of the specimen was observed and summarized, and the azimuth angle of the main crack surface was measured.

## Results and discussion

### Test results

#### *CLT crack morphology*

The crack morphology of the wood grain on the cross-section of the timber is usually divided into two types: ring shake (Fig. 4a) and heart shake (Fig. 4b). Ring shake

(a) JAW-2000 multi-channel structure test loading system

(b) AG-IC electronic universal mechanical testing machine

**Fig. 3** Testing machines of the three-point bending test and the improved planar shear test. **a** JAW-2000 multi-channel structure test loading system. **b** AG-IC electronic universal mechanical testing machine


(a) Ring shake

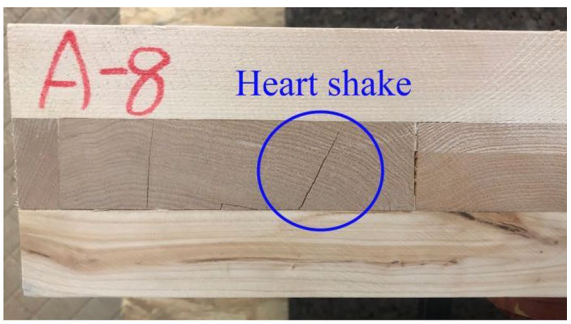


(b) Heart shake


(c) New shake which is neither ring shake nor heart shake

**Fig. 4** Crack morphology on the CLT vertical layer. **a** Ring shake, **b** heart shake, **c** new shake which is neither ring shake nor heart shake

includes the crack along the annual ring and the crack along the tangent direction of the annual ring; heart shake refers to the crack along the wood ray. In this research, except for ring shake and heart shake, there was a new crack morphology on the cross-section of the CLT vertical layer under mechanical stress, as shown in Fig. 4c.

### *CLT crack azimuth angle*

The orientation of the crack surfaces of the CLT three-point bending A, B-series specimens was symmetrical with respect to the middle of the specimens. The azimuth angle of the crack surface refers to the included angle between the crack direction and the length direction of the specimens, ranging from 0 to 90°.

Table 1 summarizes the vertical layer crack morphologies and crack azimuth angles of the CLT three-point bending A, B-series specimens and the CLT planar shear C-series specimens. For example, A4 (50°) represents the A-series specimen, the specimen number is 4, and the angle in bracket indicates that the crack azimuth angle is 50°.

From Table 1: the specimens with two cracks were A10 (25°, neither ring shake nor heart shake; 50°, heart shake), B1 (35°, heart shake; 50°, ring shake), B5 (45° and 50°, ring shake), A16 (40°, heart shake; 50°, neither ring shake nor heart shake). The specimen with three cracks was A15 (45°, ring shake; 45°, neither ring shake nor heart shake; and a crack along the wood ray—annual ring—wood ray). The number of specimens with crack azimuth angles between 40° and 50° accounted for 63.3% of the total, and that between 25°–40° or 50°–65° accounted for 23.3%.

### *Hemlock CLT planar shear strength*

Failure tests on the hemlock CLT A, B, C-series specimens were conducted to obtain the maximum load value of the load–displacement curve, and then the planar shear strength of each hemlock CLT specimen was calculated according to Eq. 1 and Eq. 2. The mean values (peak load and shear strength) are shown in Table 2.

Table 2 shows that the average shear strength of the hemlock CLT tested by the A, B-series specimens was almost the same, and the relative error was 0.8%. This result showed that in the three-point bending test, the width of the specimen had virtually no effect on the hemlock CLT shear strength. The planar shear strength of the hemlock CLT tested by the three-point bending test was quite consistent with that tested by the improved planar shear test, and the relative error was only 5.7%. The dispersion of the CLT shear strength tested by the improved planar shear test was much greater than that tested by the three-point bending test, and the coefficient of variation of the former was 24.7% while that of the latter was 10.5%.

### Stress analysis of the CLT vertical layer

In the test, the vertical layers of the CLT three-point bending specimen and the CLT shear specimen were subjected to similar forces, which caused the in-plane shear in the cross-section of the vertical layer. To explore the mechanism of planar shear and crack failure of the CLT vertical layer, the stress analysis of the vertical layer was applied to obtain the principal stress, the maximum and minimum shear stresses, as well as the normal stress and shear stress on any section. Then the test results of

**Table 1** CLT vertical layer crack morphologies and crack azimuth angles of three-point bending test and improved planar shear test

| Crack morphology | Azimuth angle of crack surface | |
|---|---|---|
| | (40°–50°) | (0°–40° or 50°–90°) |
| Ring shake | A4 (50°), A5 (40°), A6 (48°), A9 (50°), A11 (40°), A12 (45°), A14 (45°), A15 (45°), A17 (40°), B1 (50°), B5 (45°,50°) | B2 (60°), C2 (60°), C8 (30°), C9 (55°) |
| Heart shake | A10 (50°), A16 (40°), B3 (50°), C1 (40°), C4 (50°), C6 (50°), C10 (45°) | A7 (25°), A8 (65°), A13 (78°), B1 (35°), B4 (85°), C3 (30°), C7(60°), C8 (30°), C9 (60°) |
| Neither ring shake nor heart shake | A15 (45°), A16 (50°), B6 (40°) | A10 (25°), A18 (30°) |

The angle in the brackets is the azimuth angle measured on the crack surface

**Table 2** Hemlock CLT planar shear strength test value

| Test | Specimen series | Specimen quantity | Peak load /kN | CLT planar shear strength /MPa |
|---|---|---|---|---|
| Three-point bending test | A | 15 | 61.18 (10.7%) | 1.32 (10.3%) |
| | B | 6 | 42.24 (10.4%) | 1.33 (10.5%) |
| Improved planar shear test | C | 9 | 47.15 (24.7%) | 1.25 (24.7%) |

The percentage in bracket is the coefficient of variation

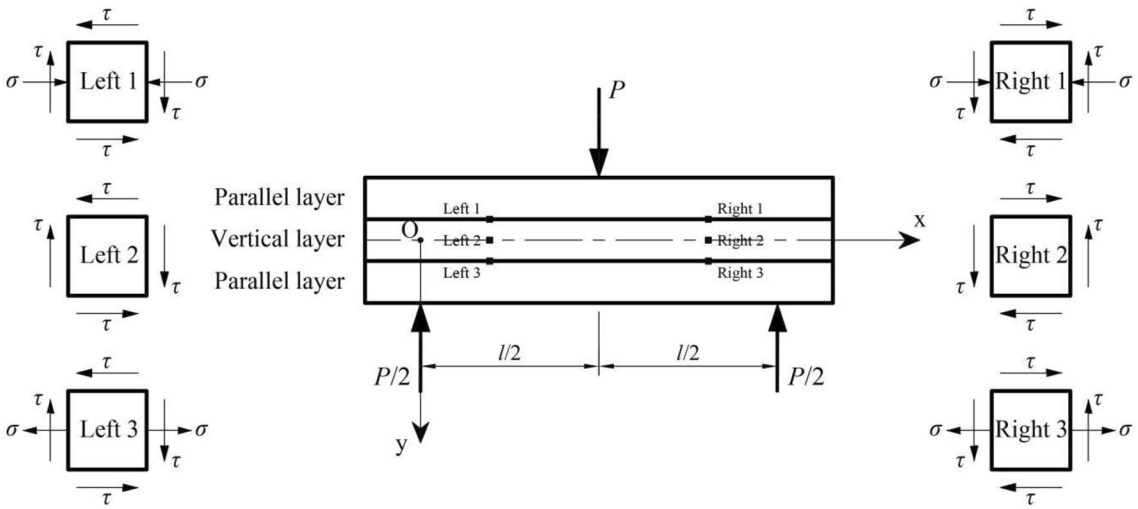


**Fig. 5** Stress components at points on the vertical layer of the CLT three-point bending specimen

the crack orientation and stress analysis were combined to reveal the failure mode of the CLT vertical layer.

The stress circle is an effective method for stress analysis [31]. The magnitude and direction of the principal stress, the maximum and minimum shear stresses, the normal stress and shear stress on each section can be accurately obtained from the stress circle.

#### *Stress analysis of the vertical layer of the CLT three-point bending specimen*

*Part I: Stress component of the vertical layer of the CLT three-point bending specimen* As shown in Fig. 5, a coordinate system O-xy was established for the CLT three-point bending specimen. The origin of the coordinates was taken at the center of the beam section at the left support. The horizontal x-axis and the vertical y-axis have positive directions.

For the CLT three-point bending specimen, three points were taken on the left half-span: left 1, left 2, and left 3, respectively, located on the upper edge, neutral axis, and lower edge of the vertical layer on the section. Similarly, three points were taken on the right half-span: right 1, right 2, and right 3. The normal stresses on the points left 1 and right 1 were the maximum compressive stress on the vertical layer of the CLT three-point bending specimen. And the normal stresses on the points left 3 and right 3 were the maximum tensile stress. The stress state at each point could be obtained by stress analysis in material mechanics: the normal stress was obtained from the bending moment analysis and the shear stress was obtained from the shear force analysis.

**Table 3** Stress state at left 1

| Stress components | Value/MPa | Direction/° |
|---|---|---|
| $\sigma_1$ | +0.613 | −47.2 |
| $\sigma_3$ | −0.711 | +42.8 |
| $\tau_1$ | +0.662 | −2.2 |
| $\tau_3$ | −0.662 | +87.8 |

**Table 4** Stress state at point B

| Stress components | Value/MPa | Direction/° |
|---|---|---|
| $\sigma_1$ | +0.547 | +48.8 |
| $\sigma_3$ | −0.714 | −41.2 |
| $\tau_1$ | +0.631 | −86.2 |
| $\tau_3$ | −0.631 | +3.8 |

Provisions on the symbol before the stress value: for normal stress, + indicates tensile stress and − indicates compressive stress; For shear stress, + indicates that it rotates counter-clockwise around the stress element (e.g., point left 1), and − indicates clockwise. Provisions on stress direction (Table 3, Table 4): when the element rotates counter-clockwise along the positive x-axis, it is +, and clockwise is −. The above provisions apply to all stress analyses in this paper.

To ensure that the stress on the CLT vertical layer was elastic stress, half of the maximum load was taken as the load for calculating the stress, as the load–displacement curve was linear when the load was less than half

of the maximum value [25]. Therefore, for the A-series specimens, the maximum tensile (compressive) stress on the vertical layer was calculated with a half load of the average maximum load 61.18 kN (Table 2), which was $P = 30.59$ kN:

$$(\sigma_x)_{\max} = 0.03457\frac{Pl}{2bh^2} = 0.1\ \text{MPa}.$$

The above formula is from reference [30], in which $l$, $b$, $h$ correspond to the relevant parameters of A-series specimens.

So the normal stresses on the x-section of left 1 and right 1 were −0.1 MPa. The normal stresses on the x-section of left 3 and right 3 were + 0.1 MPa. The points left 2 and right 2 were located on the neutral axis of the vertical layer, so the normal stresses on the x-section of them were 0.

According to Eq. 1, the shear stress of A-series specimens was 0.66 MPa. So the shear stresses on the x-section of the points left 1, left 2, and left 3 were + 0.66 MPa, and that on the y-section were −0.66 MPa. The shear stresses on the x-section of right 1, right 2, and right 3 were −0.66 MPa, and that on the y-section were + 0.66 MPa.

In Fig. 6, the stress components at left 1 were:

on the x-section: $\sigma_x = -0.1$ MPa, $\tau_{xy} = +0.66$ MPa;

on the y-section: $\sigma_y = 0$, $\tau_{yx} = -0.66$ MPa.

*Part II: Stress circle of the vertical layer of the CLT three-point bending specimen* Based on the stress components on the x, y-sections at the point left 1, the stress circle of left 1 was drawn as shown in Fig. 7. The same method can be used to draw stress circles for left 2, left 3, right 1, right 2, and right 3.

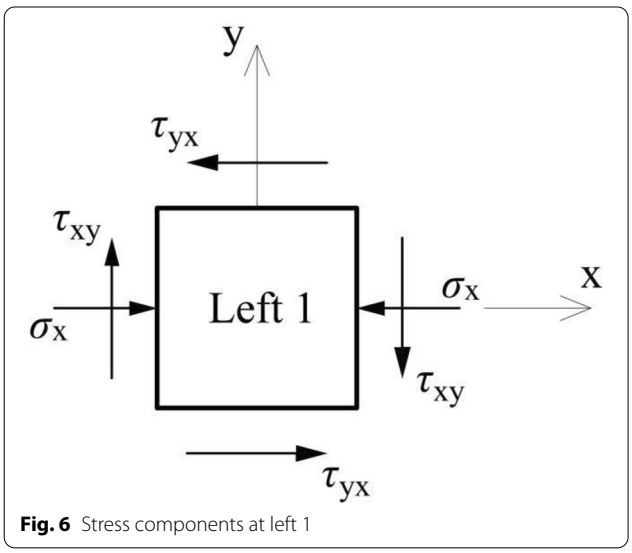


**Fig. 6** Stress components at left 1

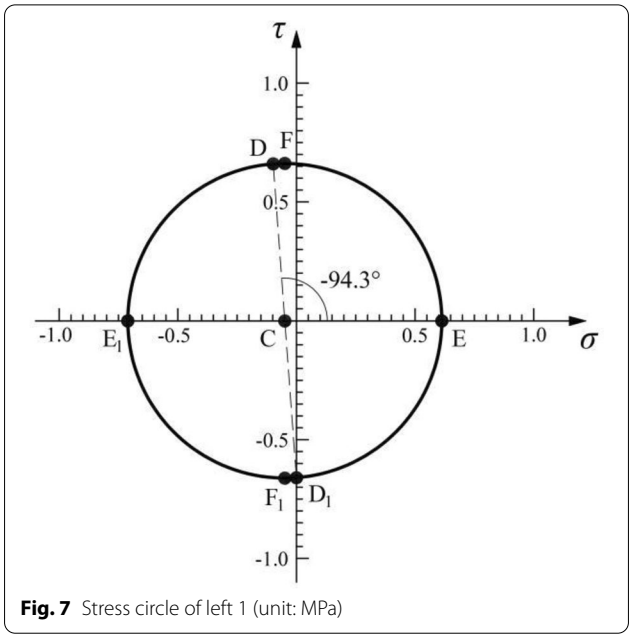


**Fig. 7** Stress circle of left 1 (unit: MPa)

*Part III: Principal stress of the vertical layer of the CLT three-point bending specimen* The values of the first principal stress and the third principal stress could be read from the abscissa of E and $E_1$, which were the intersection points of the stress circle and the σ-axis. And the corresponding principal direction could be read from the angle $\angle DCE$.

The stress circle of left 1 (Fig. 7) shows that E (+0.613, 0), $E_1$ (−0.711, 0), $\angle DCE = -94.3°$. Therefore, the principal stress and their corresponding principal directions at left 1 were as follows (Fig. 8):

$\sigma_1 = +0.613$ MPa, direction: −47.2°;

$\sigma_3 = -0.711$ MPa, direction: + 42.8°.

From the stress circles of the points left 2, left 3, right 1, right 2, and right 3, the principal stress and corresponding principal direction could be obtained similarly.

The first principal stresses at the points left 1, left 2, and left 3 of the three-point bending specimen were the tensile stress, and the angles between their direction (the direction of the normal line outside the first principal plane) and the x-axis were −42.8°, −45° and −47.2°, respectively. The first principal stresses at the points right 1, right 2, and right 3 were also tensile stress, and the angles between their direction and the x-axis were + 42.8°, + 45°, and + 47.2°, respectively.

The value of the angle between the direction of tensile stress and the x-axis on the left half-span was opposite to that on the right half-span, indicating that their first principal plane orientation was symmetrical with respect to the middle span. This was consistent with the phenomenon that the azimuth orientation of the crack surface on

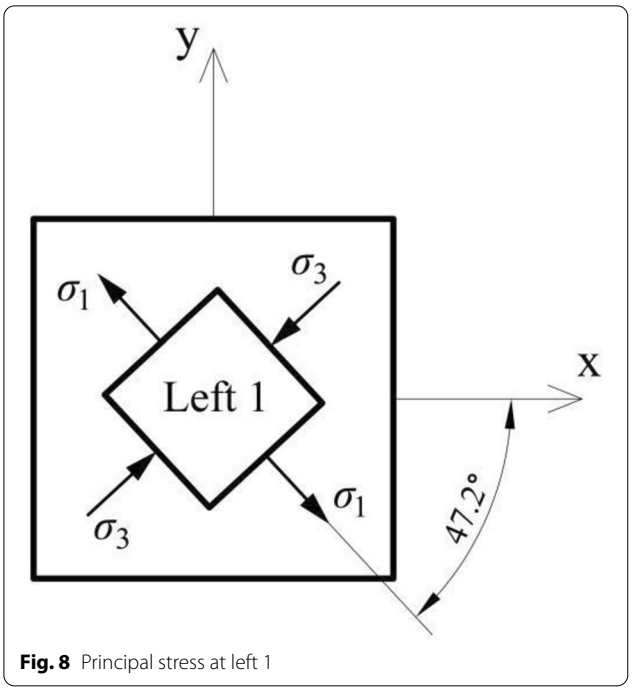


**Fig. 8** Principal stress at left 1

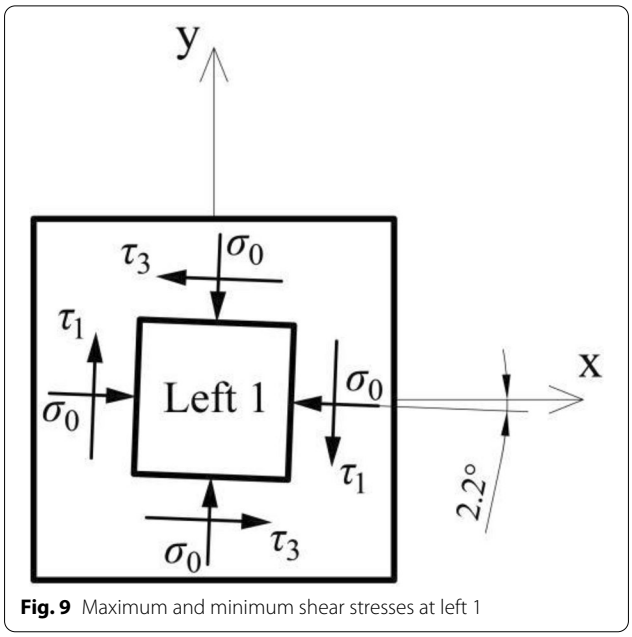


**Fig. 9** Maximum and minimum shear stresses at left 1

the vertical layer of the CLT three-point bending specimen was symmetrical with respect to the middle span.

In addition, there were points on the vertical layer of the CLT three-point bending specimen. The azimuth angle of their first principal plane only differed by 2.2° from that of the points on the neutral axis, and the difference in the magnitude of the first principal stress between the two was only 7.6%. Therefore, the stress state of the CLT vertical layer in the three-point bending test could be approximately treated as a pure shear stress state.

*Part IV: Maximum and minimum shear stresses of the vertical layer of the CLT three-point bending specimen* In Fig. 9, the values of the maximum and minimum shear stresses could be read from the ordinates of the two points F and $F_1$ with the largest distance from the stress circle to the σ-axis, which were +0.662 MPa and −0.662 MPa, respectively. The maximum shear stress $\tau_1$ was located on the cross-section that was rotated 2.2° clockwise along the positive x-axis, so the angle was −2.2°. The minimum shear stress $\tau_3$ was located on the cross-section rotated 87.8° counter-clockwise along the positive x-axis, so the angle was +87.8°.

Similarly, for the points left 2, left 3, right 1, right 2 and right 3, the maximum and minimum shear stresses could also be obtained by performing the same analysis.

The stress state (including the first principal stress $\sigma_1$, the third principal stress $\sigma_3$, the maximum shear stress $\tau_1$, the minimum shear stress $\tau_3$) at left 1 is concluded in Table 3.

**Stress analysis of the vertical layer of the CLT-improved planar shear specimen**

Point B was taken at the interface between the parallel layer and the vertical layer of the CLT shear specimen (Fig. 2). The x-section of point B was located at the interface between the parallel layer and the vertical layer. The x-axis was perpendicular to the x-section through point B, and its positive direction was along the outer normal. The y-axis was perpendicular to the x-axis, and the section perpendicular to the y-axis through point B was the y-section of point B.

The formulas for calculating normal stress and shear stress were as follows:$\sigma = P\sin\beta/bl$, $\tau = P\cos\beta/bl$.

Half of the maximum load 47.15 kN (Table 2) measured by the CLT shear test was taken to calculate the normal stress and shear stress at point B on the CLT vertical layer. According to the average value of the CLT planar shear strength 0.625 MPa and the relationship $\sigma = \tau\tan 15°(\beta = 15°)$ [25], $\sigma$ could be obtained as 0.167 MPa. In this case:

on the x-section: $\sigma_x = -0.167$ MPa, $\tau_{xy} = -0.625$ MPa;
on the y-section: $\sigma_y = 0$, $\tau_{yx} = +0.625$ MPa.

The stress components on the x, y-sections of point B are shown in Fig. 10.

Through drawing the stress circle at point B, the following values could be obtained.

In summary, the stress circle analysis of the vertical layer of the CLT three-point bending specimen and the CLT shear specimen showed that:

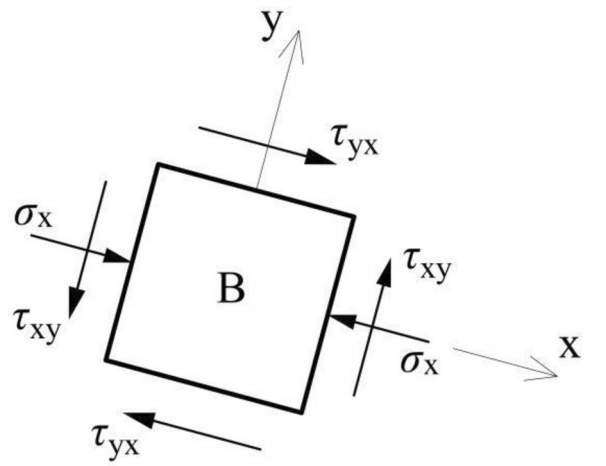


**Fig. 10** Stress components at point B

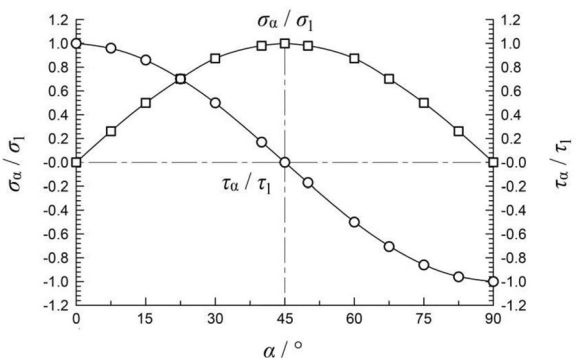


**Fig. 11** Stress distribution of the vertical layer on the *a* section under the CLT in-plane shear

1) Under the influence of the maximum normal stress on the vertical layer, the first principal stress obtained by the CLT three-point bending test was 7.6% different from that under pure shear, and the directions of these two differed by 2.2°. The maximum and minimum shear stresses obtained by the bending test were only 0.3% different from that under pure shear, and the angle between the surfaces where the two located differed by 2.2°.
2) The first principal stress obtained by the CLT-improved planar shear test was 12.5% different from that under pure shear, and the directions of these two differed by 3.8°. The maximum and minimum shear stresses obtained by the shear test were only 0.9% different from that under pure shear, and the angle between the surfaces where the two located differed by 3.8°.

The results of principal stress, maximum and minimum shear stresses obtained by the three-point bending test and the improved planar shear test showed that the points on the CLT vertical layer of these two tests could be approximated as in a pure shear stress state. Considering the accuracy of the approximation, the three-point bending test was better than the improved planar shear test.

For both the three-point bending test and the improved planar shear test, the stress circle of the CLT vertical layer in the pure shear stress state (ignoring the normal stress) was drawn, then the abscissa and ordinate of the specific points on the circumference were obtained. Figure 11 shows the normal stress $\sigma_\alpha$ and shear stress $\tau_\alpha$ of the points on the CLT vertical layer on the $\alpha$ section in a specific orientation. $\alpha$ is the angle at which the stress element rotates around the positive axis-x. Its definition is the same as the stress direction mentioned above.

#### Failure mode of the CLT vertical layer in-plane shear

In material mechanics, the mechanism analysis of the compression failure of cast-iron cylinders and the torsion failure of cast-iron circular shafts are two classic examples of combining stress analysis with the orientation of the failure section [32]. Although the compression load of the cast-iron cylinder produces compression deformation, the failure caused by it is called shear failure, instead of compression failure. And although the torsion of the cast-iron shaft produces torsional shear deformation, the failure caused by it is called tensile failure, instead of torsional failure. In other words, the type of deformation cannot determine the type of failure. Therefore, in the CLT three-point bending test and the CLT-improved planar shear test, the in-plane shear deformation of the vertical layer could not be simply considered as shear failure.

#### *CLT vertical layer crack azimuth angle in the range of 40°–50°*

A total of 30 three-point bending specimens and planar shear specimens were tested. After the test, there were 19 specimens with crack azimuth angles of the vertical layer between 40° and 50°, accounting for 63.3% of the total number (Table 1).

The principal stress analysis of the CLT vertical layer showed that when the three-point bending test achieved the CLT vertical layer in-plane shear, the first principal stress was tensile, and the orientation of its action surface (first principal plane) was between −42.8° and −47.2° on the left half-span, and between + 42.8° and + 47.2°on the right half-span. The signs reflected that the first principal plane of the vertical layer was symmetrical on the left half-span and right half-span. When the improved planar shear test achieved the CLT vertical layer in-plane shear, the first

principal stress was also the tensile stress, and the orientation of its action surface was + 48.8° or −48.8°. This showed that whether it was a three-point bending test or an improved planar shear test, the azimuth angle of the first principal plane of each point on the CLT vertical layer was between 40° and 50°, which indicated that the CLT vertical layer was cracked under planar shear. The agreement between the azimuth angle of the crack surface and the azimuth angle of the first principal plane of the CLT vertical layer reached 63.3%.

For the local stress $\sigma_\alpha$ and $\tau_\alpha$ on the crack surface of the vertical layer with the crack angle in the range of 40–50°, $\sigma_\alpha/\sigma_1$ changed from 0.98 to 1, $\tau_\alpha/\tau_1$ changed from 0.17 to 0 (Fig. 11). Although the vertical layer was approximately in pure shear and underwent shear deformation, since $\tau_\alpha$ was very small, it could not cause the vertical layer to crack along the $\alpha$ plane, so the corresponding failure could not be called shear failure. On the other hand, $\sigma_\alpha$ was very large, almost equal to the first principal stress, and it was also tensile stress. Based on these two findings, it could be considered that the failure of CLT was related to the stretching of the horizontal wood grain of the vertical layer. And within this angle range, the failure mode of CLT was tensile failure.

According to the above analysis, the failure mode of C1 specimen (Fig. 12) could be explained as follows.

There were two cracks on the vertical layer of the CLT shear specimen C1. One of the cracks was at the interface, and the wood chips were clearly visible on the cracked interface, so the crack occurred along the interlayer rather than the glue layer. The azimuth angle of another crack was 40°, so it was under tensile failure.

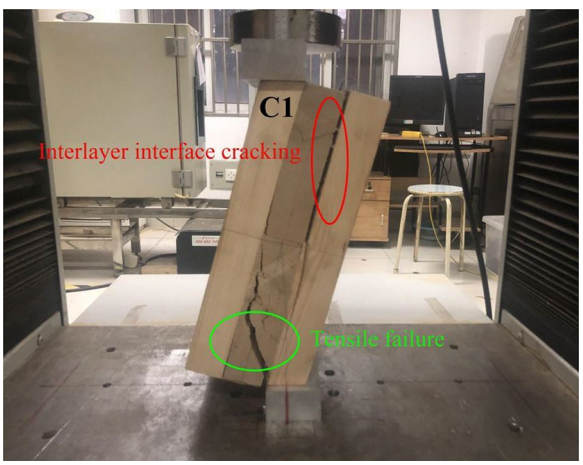


**Fig. 12** Crack surface and its failure type on the CLT shear specimen C1

#### *CLT vertical layer crack azimuth angle in the range of 0°–22.5° or 67.5°–90°*

The local stress $\sigma_\alpha$ and $\tau_\alpha$ on the crack surface on the vertical layer with crack angle in the range of 0°–22.5° or 67.5°–90° changed as follows: $\sigma_\alpha/\sigma_1$ changed from 0 to 0.71, $\tau_\alpha/\tau_1$ changed from 1 to 0.71. When $\tau_\alpha$ was large, and the vertical layer cracked along the action plane of the shear stress, the CLT failure could be considered as shear failure. The corresponding specimens were as follows: A13 (with an azimuth angle of 78°) and B4 (with an azimuth angle of 85°).

#### *CLT vertical layer crack azimuth angle in the range of 22.5°–40° or 50°–67.5°*

The specimens with the vertical layer crack angle within this range were: A7 (25°, along the wood ray), A8 (65°, along the wood ray), A10 (25°, neither along the annual ring nor along the wood ray), A18 (30°, along the annual ring tangent, connecting the wood ray), B1 (35°, the wood grain was not clear), B2 (60°, the annual ring line was blurred), C8 (two cracks: 30°, along the wood ray; 30°, along the annual ring), C9 (two cracks: 60°, along the wood ray; 55°, along the annual ring), 9 pieces in total. It should be noted that the definition of direction here is related to the crack morphology. For example, "along the wood ray" means the same as "heart shake". See the definitions of different crack morphologies for more details.

For the local stress of the vertical layer crack angle within this range, $\tau_\alpha/\tau_1$ decreased fastly from 0.71 to 0.17, and the value was not very large. Therefore, it cannot be called shear failure. $\sigma_\alpha/\sigma_1$ changed from 0.71 to 0.98. Although $\sigma_\alpha$ was relatively large and slowly increased as the azimuth angle increased, it was not certain that this phenomenon was due to tensile failure. This situation just reflected the limitation of applying stress analysis for the failure of the vertical layer with the crack angle in the range of 22.5°–40° or 50°–67.5°. Perhaps it was necessary to combine the characteristics of wood as an anisotropic material and make further analysis of the microstructure of the wood.

As the tensile property of wood ray was worse than that of nearby wood fibers, it can be considered that the failure of cracks of the following six specimens was caused by tensile stress: A7, A8, A18, C8 (30°, along the wood ray), C7, C9 (60°, along the wood ray). However, the reason for the failure of cracks of the following specimens could not be determined yet: A10, B1, B2, C8 (30°, along the annual ring), C9 (55°, along the annual ring).

In summary, the specimens with the azimuth angle of the crack surface of 40°–50° accounted for 63.3% of the total number. The specimens with the azimuth angle of 22.5°–40° or 50°–67.5° along wood rays accounted for

20%. These two cases account for 83.3% of the total number of specimens, indicating that the failure of the specimens was related to the transverse tensile property of the cross-section of the vertical layer. The specimens with the azimuth angle of 0°–15° or 75°–90° along wood rays only accounted for 6.7%, and the failure mode of them was shear failure.

## Conclusions

According to the crack morphologies and shear strength test results of the three-point bending test and improved planar shear test, this paper carried out the research on the in-plane shear failure mode of CLT panel. The stress state of the CLT vertical layer was determined by analyzing the principal stress, maximum and minimum shear stresses of the point on the vertical layer through stress circle. And the failure mechanism of the vertical layer was comprehensively analyzed by combing planar stress state and crack azimuth angle. The main conclusions were as follows:

1. The planar shear strength of CLT measured by the three-point bending test was highly consistent with that measured by the improved planar shear test. The dispersion of CLT shear strength obtained by the improved planar shear test was greater than that measured by the three-point bending test.
2. CLT vertical layer in-plane shear of the three-point bending test and improved planar shear test could be treated as pure shear. For the accuracy of the approximation, the three-point bending test was better than the improved planar shear test.
3. For the CLT vertical layer in the three-point bending test and improved planar shear test, the orientation of the crack surface was in good agreement with that of the first principal plane, and the number of coincided specimens accounted for 63.3% of the total.
4. There were two failure modes in the CLT vertical layer in-plane shear: tensile failure and shear failure. In this study, 83.3% of the specimens were under tensile failure and 6.7% of the specimens were under shear failure.

In this paper, the planar shear strength test and failure mechanism analysis of three-layer CLT panel with equal thickness were carried out. In the future, it is planned to carry out relevant research on three-layer CLT panel with unequal thickness and five, seven-layer CLT panel, so as to improve the systematicness and integrity of the research on the in-plane shear failure mechanism of CLT panel. The reason why the coefficient of variation of the three-point bending test was smaller than that of the improved planar shear test needs to be further explored. Moreover, the crack morphologies of some specimens in this paper have not been fully explained. In the follow-up study, it will be further analyzed combined with the orthotropy characteristic of wood and the mesostructure of wood.

**Abbreviations**

CLT: Cross-laminated timber; MC: Moisture content; PUR: Polyurethane.

**Acknowledgements**

The authors would like to thank Mr. Gongxun Ma (Nanjing Tech University, China) for his assistance with the theoretical support.

**Author contributions**

YZ contributed to experiments, data analysis, and writing the manuscript. ZS contributed to experiments. HL contributed to data analysis. YL contributed to manuscript review and editing. ZW designed this study and contributed to manuscript revision and funding acquisition. All authors read and approved the final manuscript.

**Funding**

This work was sponsored by the Science and Technology Project for Policy Guidance of Jiangsu Province (SZ-LYG 2020016).

**Availability of data and materials**

The datasets used and analyzed during this study are available from the corresponding author upon reasonable request.

## Declarations

**Competing interests**

The authors declare that they have no competing interests.

**Author details**

[1]College of Materials Science and Engineering, Nanjing Forestry University, Nanjing 210037, China. [2]College of Civil Engineering, Nanjing Forestry University, Nanjing 210037, China.

Received: 23 May 2022 Accepted: 8 June 2022
Published online: 18 June 2022

**References**

1. Zhou K, Li HT, Hong CK, Ashraf M, Sayed U, Lorenzo R, Corbi I, Corbi O, Yang D, Zuo YF (2021) Mechanical properties of large-scale parallel bamboo strand lumber under local compression. Constr Build Mater 271:121572. https://doi.org/10.1016/j.conbuildmat.2020.121572
2. Tan C, Li HT, Ashraf M, Corbi I, Corbi O, Lorenzo R (2021) Evaluation of axial capacity of engineered bamboo columns. J Building Eng 34:102039. https://doi.org/10.1016/j.jobe.2020.102039
3. Corbi I, Corbi O, Li HT (2020) Convolutive PD controller for hybrid improvement of dynamic structural systems. Soil Dyn Earthq Eng 137:106255. https://doi.org/10.1016/j.soildyn.2020.106255
4. Karacabeyli E, Douglas B (2013) CLT Handbook: cross-laminated timber. FPInnovations, Pointe-Claire
5. Sun JP, Niederwestberg J, Cheng FC, Chui YH (2020) Frequencies prediction of laminated timber plates using ANN approach. J Renew Mater 8(3):319–328. https://doi.org/10.32604/jrm.2020.08696
6. Muñoz F, Tenorio C, Moya R, Navarro-Mora A (2022) CLT fabricated with *Gmelina arborea* and *Tectona grandis* wood from fast-growth forest plantations physical and mechanical properties. J Renew Mater 10(1):1–17. https://doi.org/10.32604/jrm.2022.017392
7. van de Lindt JW, Furley J, Amini MO, Pei SL, Tamagnone G (2019) Experimental seismic behavior of a two-story CLT platform building. Eng Struct 183:408–422. https://doi.org/10.1016/j.engstruct.2018.12.079

8. Sandoli A, D'Ambra C, Ceraldi C, Calderoni B, Prota A (2021) Role of perpendicular to grain compression properties on the seismic behaviour of CLT walls. J Building Eng 34:101899. https://doi.org/10.1016/j.jobe.2020.101889
9. Sandoli A, D'Ambra C, Ceraldi C, Calderoni B, Prota A (2021) Sustainable cross-laminated timber structures in a seismic area: overview and future trends. Applied Science 11(5):2078. https://doi.org/10.3390/app11052078
10. Wang ZH, Wang Z, Wang BJ, Wang YL, Rao X, Liu B, Wei PX, Yang Y (2014) Dynamic testing and evaluation of modulus of elasticity (MOE) of SPF dimension lumber. BioResources 9(3):3869–3882. https://doi.org/10.15376/biores.9.3.3869-3882
11. Wang ZH, Wang YL, Cao Y, Wang Z (2016) Measurement of shear modulus of materials based on the torsional mode of cantilever plate. Constr Build Mater 124:1059–1071. https://doi.org/10.1016/j.conbuildmat.2016.08.104
12. Ding FL, Zhuang ZL, Liu Y, Jiang D, Yan XA, Wang ZG (2020) Detecting defects on solid wood panels based on an improved SSD algorithm. Sensors 20(18):5315. https://doi.org/10.3390/s20185315
13. Yoshihara M, Maruta M (2021) Effect of specimen configuration and orthotropy on the Young's modulus of solid wood obtained from a longitudinal vibration test. Holzforschung 75(5):428–435. https://doi.org/10.1515/hf-2020-0115
14. Sandoli A, Calderoni B (2020) The rolling shear influence on the out-of-plane behavior of CLT panels: a comparative analysis. Buildings 10(3):42. https://doi.org/10.3390/buildings10030042
15. Pang SJ, Jeong GY (2019) Effects of combinations of lamina grade and thickness, and span-to-depth ratios on bending properties of cross-laminated timber (CLT) floor. Constr Build Mater 222:142–151. https://doi.org/10.1016/j.conbuildmat.2019.06.012
16. Lim H, Tripathi S, Li MH (2020) Rolling shear modulus and strength of cross-laminated timber treated with micronized copper azole type C (MCA-C). Constr Build Mater 259:120419. https://doi.org/10.1016/j.conbuildmat.2020.120419
17. He MJ, Sun XF, Li Z, Feng W (2020) Bending, shear, and compressive properties of three- and five-layer cross-laminated timber fabricated with black spruce. J Wood Sci 66(1):38. https://doi.org/10.1186/s10086-020-01886-z
18. Ukyo S, Miyatake A, Hiramatsu Y (2021) Shear strength properties of hybrid (*hinoki cypress* and *Japanese cedar*) cross-laminated timber. J Wood Sci 67(1):23. https://doi.org/10.1186/s10086-021-01954-y
19. Ehrhart T, Brandner R, Schickhofer G, Frangi A (2015) Rolling shear properties of some European timber species with focus on cross-laminated timber (CLT): test configuration and parameter study. In: International Network on Timber Engineering Research: Proceedings of the 48th Meeting, Sibenik, Croatia. August 24–27, 2015. pp 61–76
20. Li MH (2017) Evaluating rolling shear strength properties of cross-laminated timber by short-span bending tests and modified planar shear tests. J Wood Sci 63(4):331–337. https://doi.org/10.1007/s10086-017-1631-6
21. Ma YX, Musah M, Si RZ, Dai QL, Xie XF (2021) Integrated experimental and numerical study on flexural properties of cross laminated timber made of low-value sugar maple lumber. Constr Build Mater 280:122508. https://doi.org/10.1016/j.conbuildmat.2021.122508
22. Li Y, Lam F (2016) Low cycle fatigue tests and damage accumulation models on the rolling shear strength of cross-laminated timber. J Wood Sci 62:251–262. https://doi.org/10.1007/s10086-016-1547-6
23. Lam F, Li Y, Li M (2016) Torque loading tests on the rolling shear strength of cross-laminated timber. J Wood Sci 62:407–415. https://doi.org/10.1007/s10086-016-1567-2
24. Wang ZH, Ghanem R (2021) An extended polynomial chaos expansion for PDF characterization and variation with aleatory and epistemic uncertainties. Comput Methods Appl Mech Eng 382:113854. https://doi.org/10.1016/j.cma.2021.113854
25. Huang YJ, Zhang YF, Wang Z, Dauletbe A, Lu Y (2022) Analysis of crack expansion and morphology of cross-laminated timber planar shear test. J Renew Mater 10(3):849–870. https://doi.org/10.32604/jrm.2022.018515
26. ASTM Standard D2718 (2011) Standard test methods for structural panels in planar shear (rolling shear). ASTM International, PA
27. EN Standard 408 (2003) Timber Structures-structural timber and glued laminated timber-determination of some physical and mechanical properties. European Committee for Standardisation, Brussels
28. Gong M, Tu D, Li L (2015) Planar shear of hardwood cross layer in hybrid cross laminated timber. In: 5th International Scientific Conference on Hardwood Processing, Quebec City. September 15–17, 2015. pp 85–90
29. ASTM Standard D198 (2015) Standard test methods of static tests of lumber in structural sizes. ASTM International, PA.
30. Wang Z, Lu Y, Xie WB, Gao ZZ, Ding YW, Fu HY (2019) Shear stress analysis and interlayer shear strength test of Cross Laminated Timber (CLT) Beam (in Chinese). Scientia Silvae Sinicae. 55(2):152–158. https://doi.org/10.11707/j.1001-7488.20190216
31. Babaeeian M, Mohammadimehr M (2021) Experimental and computational analyses on residual stress of composite plate using DIC and Hole-drilling methods based on Mohr's circle and considering the time effect. Opt Lasers Eng 137:106355. https://doi.org/10.1016/j.optlaseng.2020.106355
32. Hibbeler RC (2016) Mechanics of materials, 10th edn. Prentice Hall, Hoboken


## Publisher's Note